Intrinsic Stress of Eutectic Au/Sn Die Attachment and Effect on Mode-Matched MEMS Gyroscopes

Brenton R. Simon, Gunjana Sharma, Sergei A. Zotov, Alexander A. Trusov, Andrei M. Shkel
MicroSystems Laboratory, University of California, Irvine, CA, USA

***Abstract*— We report on the intrinsic stress imparted to MEMS gyroscopes and the effects on frequency mismatch due to high-temperature die attachment processes, such as eutectic Au/Sn solder. The resonant frequencies of a number of symmetric MEMS gyroscopes are characterized before and after die attachment, along with X-ray imaging to observe the random solder reflow that occurred during attachment. Frequency shift is observed and compared to the die attachment area, with an 87 percent correlation to the length of the solder reflow. A model of the phenomena is presented with less than 0.1 percent agreement to the experimental results, indicating an optimal die attachment for the minimization of stress-induced frequency changes.**

I. Introduction

High-performance MEMS gyroscopes require high Q-factor, small frequency mismatch, and high temperature robustness. These requirements not only provoke many challenges in the design, fabrication, and control of these sensors, but also packaging. Packaging must provide a high-level of vacuum to maximize the Q-factor of the resonate device [1], along with the prevention of stress accumulation, which can influence the drift of the resonance frequency with respect to temperature [2]. While wafer-level vacuum sealing is becoming a promising option to address both of these concerns [3], this method does not allow for sealing with getter material, minimizing the vacuum-level that can be achieved [4]. To date, the inclusion of getter material has required a separate sealing process, requiring sensor attachment to an external package.

While many bonding materials exist, there are two main options: room-temperature organic adhesives, or high-temperature solder. Organic adhesives are commonly used for low-performance applications and out-gas when exposed to vacuum, limiting Q-factor. In comparison, fluxless solders exist which out-gas little, making them excellent for vacuum applications; however, high temperatures are required to bond, potentially resulting in residual thermal stress which, when bonded asymmetrically, can not only affect the frequency mismatch, but also how frequency shift responds to temperature.

Frequency drifts can have a substantial effect on sensor performance [5]; therefore, much work has been done in order to reduce the natural frequency drifts of silicon through the use of composite structures [6], [7], as well as using temperature-dependant axial force [8]. In this paper, we show that by carefully controlling the size of the attachment area using fluxless solder, the influence of thermal stresses can be controlled. This control can either be used to reduce the overall stress from die attachment, or as a mechanical thermal compensation technique for reducing the device's thermal coefficient of resonant frequency (TCF).

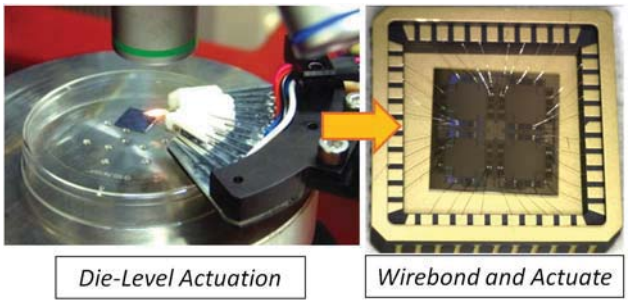

(a) Photographs showing device actuation before and after die attachment.

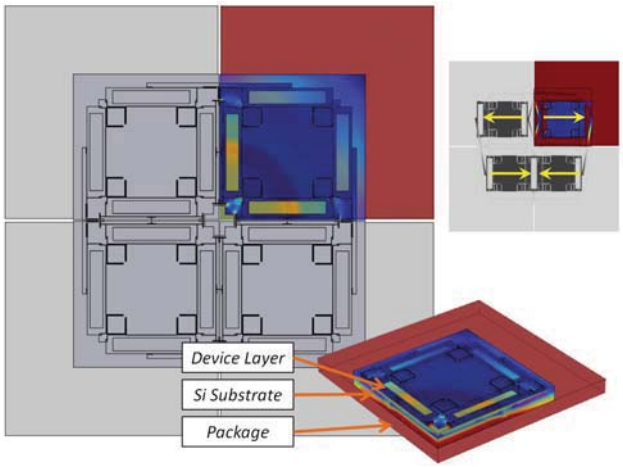

(b) 3-D Comsol model, confirming experimental results.

Fig. 1. Experimental setups and modeling.

II. Pre-Attachment Resonance Characterization

A. Gyroscope Design and Fabrication

For this experimental study, an existing, high-performance sensor design was used: a Quadruple Mass Gyroscope (QMG) [1]. The device is X-Y symmetric and consists of four resonant masses, each coupled to one another with levering structures designed to force an ideal anti-phase motion, Figure 1(b) [9]. The 2-DOF motion of each mass is reduced to single axes through the use of four shuttling structures placed around each mass. These shuttles anchor each resonant mass to the substrate at each of the four corners, Figures 6 and 8. Capacitive, differential parallel-plate electrodes are also placed on each

978-1-4799-0916-2/14/$31.00 ©2014 IEEE

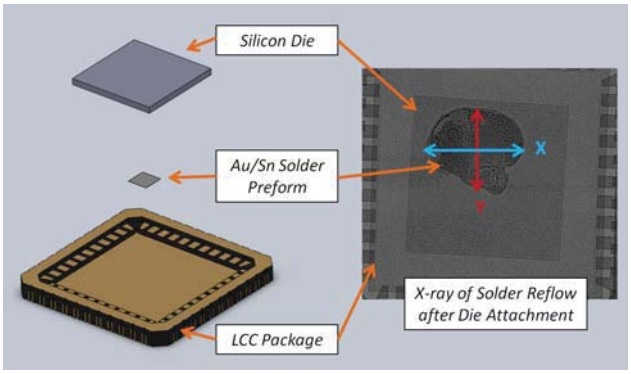

Fig. 2. Rendering of silicon die, Au/Sn solder perform and LCC package stack assembled during die attachment (left), along with X-ray image of the physical device after die attachment, showing solder reflow for quantitative measurement (right).

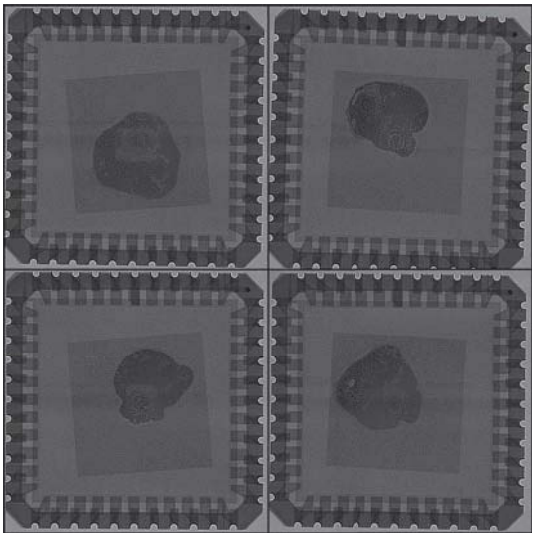

Fig. 3. Additional x-ray images showing random solder reflow. The die attachment procedure was identical in each case.

shuttle, used for both actuation and detection of the resonant structure. The devices were fabricated using a Silicon-On-Insulator (SOI) fabrication process with device layer thickness of 100 microns, buried silicon dioxide layer of 5 microns, and substrate thickness of 500 microns. In addition, a metal bonding layer was applied to the back of the device consisting of 5000 Å of gold with a 500 Å chrome adhesion layer.

B. Capacitive Resonance using Probe Card

Measuring frequency prior to packaging was completed using the integrated capacitive electrodes, interfaced through the use of an external probed card, Figure 1(a). The probe card interfaced all four sets of differential electrodes on a single mass of the resonant structure. Because the device consists of four masses, each with 2-DOF, a total of eight principal resonances exist, four along each axis. Under typical device operation, all four masses are selectively actuated with either positive or negative polarity to reflect the desired anti-phase mode of resonance. While this technique isolates a single mode of resonance, actuating only a single mass allows for the observation of all four modes along each axis, examples of which are shown in Figure 4.

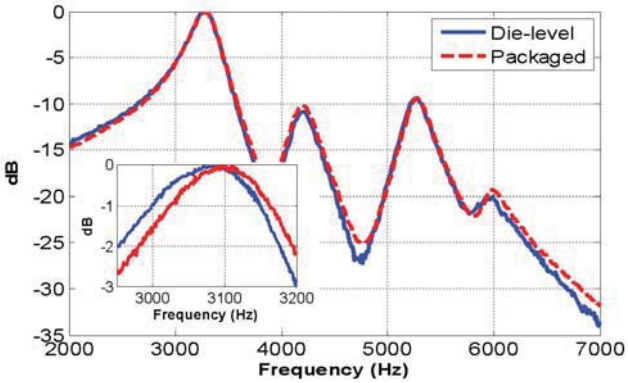

Fig. 4. Capacitive frequency sweeps before and after die attachment, showing change in frequency due to internal stress imparted during die attachment.

III. Post-Attachment Resonance Characterization

A. Die Attachment Procedure

After measuring the initial resonance frequencies of both device axes by probe, sensors were packaged into symmetric, Leadless Chip Carrier (LCC) packages. The package material consisted of gold plated Kyocera A440, with material properties given in Table IV. The bonding material was a 2mm square of 80/20 Au/Sn solder, with thickness of 50 microns. Temporary graphite inserts were also used to both center the gyroscope in the package, as well as allow for a weight to be applied on top to assure good contact for bonding.

Prior to bonding, both the package and gyroscope were baked under vacuum for two hours at 350°C, releasing any residual absorbed gas. The package, solder, gyroscope, and weight were then assembled, Figure 2, placed under vacuum, and heated to the solder's eutectic point of 280°C. Once cooled, the weight and graphic inserts were removed and the electrodes of the gyroscope were wirebonded to the package leads, Figure 1(a).

B. X-ray Imaging of Solder Reflow

In order to inspect the result of the die attachment procedure, x-ray inspection was performed to identify any voids from the bonding process, as well as observe the reflow of the solder. Despite the fabricated square shape of the solder preform, uncontrolled reflow of this material creates an asymmetric circular attachment area beneath the device. In an effort to quantify this behavior, the final solder dimensions were measured along both axes of resonance for each tested device, as shown in Figure 2. Additional examples of the variability of the reflow process are shown in Figure 3.

C. Capacitive Resonance through Packaging

The gyroscope was then capacitively actuated and detected through the package. For an accurate comparison to the pre-attachment results, the same mass was resonated, producing

TABLE I

MATERIAL PROPERTIES

Parameter	Silicon	Kyocera A440	Units
Density	2329	3800	kg/m^3
Young's Modulus	170	310	GPa
Poisson's Ratio	0.28	0.23	-
Coefficient of Thermal Expansion	2.6	7.1	ppm/K

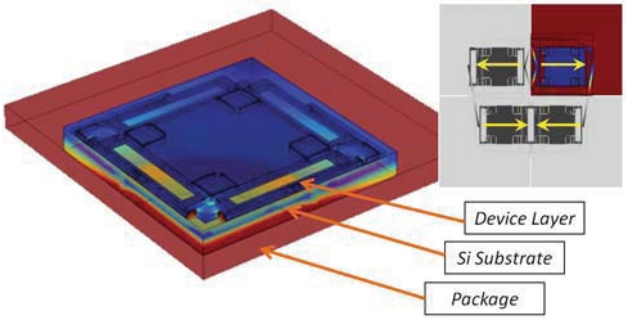

Fig. 5. 3-D Comsol model of 1/4 of the device. Stress due to die attachment was solved, along with the effect on the anti-phase resonance frequency.

a comparable resonance sweep as initially identified. A slight frequency shift was observed after packaging. Figure 4 shows a comparison of the frequency spectrum observed before and after die attachment, with inset displaying the useful anti-phase resonance frequency, highlighting the induced frequency shift.

For each axis of resonance, the observed frequency shift was plotted versus the final solder length along the axis in question. This data is plotted in Figure 7. A linear relationship can be observed between these two parameters with an 87 percent correlation, showing the influence of bonding stress on the final observed mechanical resonance of the device.

IV. FINITE ELEMENT MODELING

A. Modeling Parameters

In order to form a predictive model of the observed behavior, a 3-D Finite Element Model was created consisting of one quarter of the device and package, Figure 5. Symmetry of both the resonant structure and packaging allowed for the reduction of the model to only one of the four proof masses with appropriate symmetric and anti-symmetric boundary condition. The modeled layers included the resonant device layer, silicon substrate, and ceramic package, along with the interfaces between each [10]. The modeling consisted of two stages: 1) calculate the internal stress due to the thermal mismatch between the silicon and ceramic when temperature is decreased from 280°C to 25°C, and 2) determine the anti-phase resonant frequency as a result of this additional stress. These final resonant frequencies were then compared to the initial frequency of the device, before bonding to the substrate at elevated temperatures. The relevant material properties used for both the silicon device and packaging are given in Table I. This core model allowed for the manipulation of the bonding area between the silicon substrate and packaging, for the

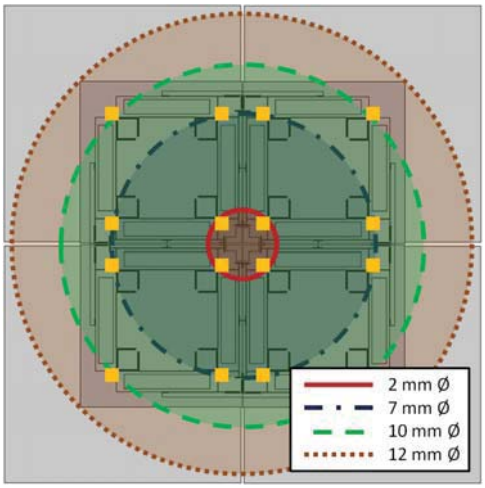

Fig. 6. The diameter of the die attachment in the model was incremented every 0.5mm, with critical diameters shown above when the die attachment reached a position directly below device anchors (shown in yellow).

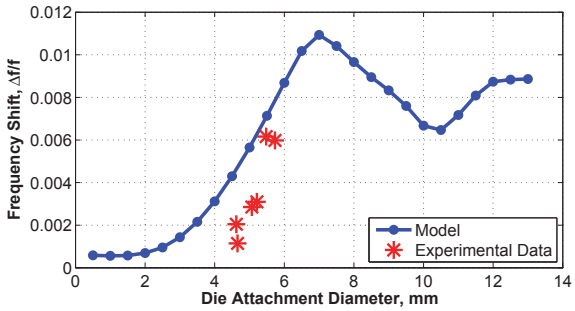

Fig. 7. Frequency shift versus die attachment size for the experimental data and model, showing good agreement. The critical diameters from Figure 5 coincide with distinct changes in how frequency is affected by increasing die attachment diameter. Mismatch between model and experiment is believed to be due to an irregular shape of attachment.

purpose of observing the effect on resonant frequency. Using this model, two different forms of symmetric die attachment were analyzed: a central, circular attachment area, and frame around the edge of the device, both of varying width.

B. Central Die Attachment

The attachment of the silicon substrate to the ceramic package was varied by geometry and dimensions, but first chosen as a circle placed in the center of the device. The attachment diameter was varied every 0.5mm, from 0.5mm to 13mm. Figure 6 displays several critical die attachment diameters, in relation to the device. The anchors attaching the device layer to the substrate are highlighted in yellow.

When comparing the modeled frequency shift versus attachment diameter, Figure 7, critical points can be observed in the plot coinciding with the anchors of the resonant structure. The frequency shift due to stress is lowest when the solder is restricted to within the four center anchors of the device and reaches a maximum value of 1 percent when it has encompassed half the device anchors. The experimental data

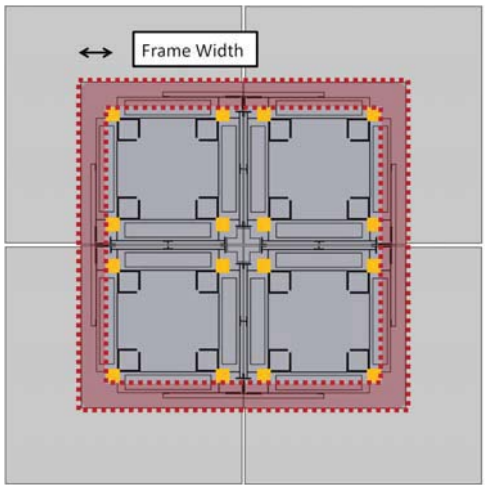

Fig. 8. Diagram of the frame-type die attachment geometry.

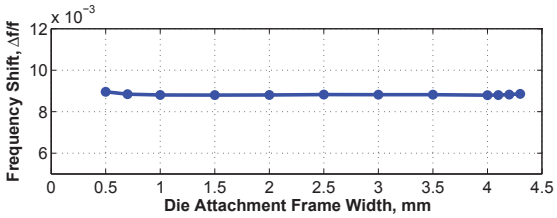

Fig. 9. Frequency shift versus die attachment size for the frame-type geometry die attachment model.

is also displayed, showing a variation in the frequency shift from 0.1-0.6 percent when using an identical die attachment procedure, indicating a potential 0.5 percent frequency split due to uncontrolled, asymmetric die attachment alone.

C. Frame Die Attachment

A second form of attachment geometries was also modeled: an external frame around the outer boarder of the device. Figure 8 shows an example of this geometry and how the dimensions were iterated. Frequency shift data from the model is shown in Figure 9, which displays roughly a constant value with increasing width of the frame. The value of this frequency shift compared to the initial frequency is approximately 0.9 percent, and is identical to that of the circular attachment when all of the device anchors have been encompassed.

V. Conclusion

From the model, it is shown that by restricting the attachment area to within a single, central anchored area of the resonant structure, a low absolute change in frequency is predicted to less than 0.1 percent, as well as reduced sensitivity to variation in die attachment size. This low shift in frequency reflects reduced stress imparted to the silicon device from the ceramic package. This can also be observed when examining the corresponding TCF for devices with reduced die attachment size, Figure 10. With reduced size, the TCF of the device more accurately reflects that of the innate TCF of silicon. As die attachment increases, so does the TCF,

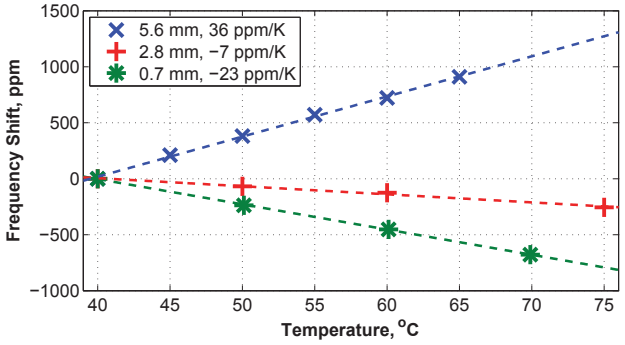

Fig. 10. Experimental thermal coefficient of frequencies of QMGs with various die attachment sizes. As die attachment increases, TCF shifts from a negative to positive value.

eventually even becoming a positive drift. This trend shows that while stress due to die attachment can be minimized through device design and packaging, if controlled adequately, it can also be used as a form of thermal compensation.

Acknowledgment

This work was supported by the ONR/NSWCDD grants N00014-09-1-0424 and N00014-11-1-0483. Devices were designed, modeled, and characterized at the UC Irvine MicroSystems Laboratory. Fabrication was performed at the UC Irvine Integrated Nanosystems Research Facility and UC Los Angeles Nanolab.

References

[1] A.A. Trusov, I.P. Prikhodko, S.A. Zotov, A.R. Schofield, A.M. Shkel, "Ultra-High Q Silicon Gyroscopes with Interchangeable Rate and Whole Angle Modes of Operation," IEEE Sensors 2010 Conference, Waikoloa, HI, USA, November 1-4, 2010.

[2] E. Tatar, C. Guo, T. Mukherjee, G.K. Fedder, "Interaction Effects of Temperature and Stress on Matched-Mode Gyroscope Frequencies," Transducers 2013 Conference, 2013.

[3] R.N. Candler, M.A. Hopcroft, B. Kim, W.-T. Park, R. Melamud, M. Agarwal, G. Yama, A. Partridge, M. Lutz, T.W. Kenny, "Long-Term and Accelerated Life Testing of a Novel Single-Wafer Vacuum Encapsulation for MEMS Resonators," IEEE J. Microelectromech. Syst., Vol. 15, No. 6, pp. 1446-1456, 2006.

[4] I.P. Prikhodko, B.R. Simon, G. Sharma, S.A. Zotov, A.A. Trusov, A.M. Shkel, "High and Moderate Level Vacuum Packaging of Vibratory MEMS," 46-th International Symposium on Microelectronics (IMAPS 2013), Orlando, FL, USA, September 30 - October 3, 2013.

[5] I.P. Prikhodko, A.A. Trusov, A.M. Shkel, "Compensation of drifts in high-Q MEMS gyroscopes using temperature self-sensing," Sensors and Actuators A: Physical, Vol. 201, pp. 517-524, October 2013.

[6] R. Melamud, S.A. Chandorkar, B. Kim, H.K. Lee, J.C. Salvia, G. Bahl, M.A. Hopcroft, T.W. Kenny, "Temperature insensitive composite micromechanical resonators," IEEE J. Microelectromech. Syst., Vol. 18, No. 6, pp. 14091419, 2009.

[7] R. Tabrizian, G. Casinovi, F. Ayazi, "Temperature-Stable Silicon Oxide (SilOx) Micromechanical Resonators," IEEE Transactions on Electron Devices, Vol. 60, No. 8, August 2013.

[8] W.T. Hsu, J.R. Clark, C.T.-C. Nguyen, "Mechanically temperature-compensated flexural-mode micromechanical resonators," IEDM Tech. Dig., 2000, pp. 399-402.

[9] B.R. Simon, A.A. Trusov, A.M. Shkel, "Anti-Phase Mode Isolation in Tuning-Fork MEMS using a Lever Coupling Design," IEEE Sensors 2012 Conference, Taipei, Taiwan, October 28 31, 2012.

[10] S.S. Walwadkar, J. Cho, "Evaluation of Die Stress in MEMS Packaging: Experimental and Theoretical Approaches," IEEE Transactions on Components and Packaging Technologies, Vol. 29, No. 4, December 2006.